TOXICOLOGICAL SCIENCES **118(1)**, 160–170 (2010)
doi:10.1093/toxsci/kfq244
Advance Access publication August 16, 2010

Silver Nanoparticle Induced Blood-Brain Barrier Inflammation and Increased Permeability in Primary Rat Brain Microvessel Endothelial Cells

William J. Trickler,* Susan M. Lantz,* Richard C. Murdock,† Amanda M. Schrand,† Bonnie L. Robinson,* Glenn D. Newport,* John J. Schlager,† Steven J. Oldenburg,‡ Merle G. Paule,* William Slikker, Jr.,* Saber M. Hussain,† and Syed F. Ali*,[1]

*Neurochemistry Laboratory, Division of Neurotoxicology, National Center of Toxicological Research/Food and Drug Administration, Jefferson, Arkansas 72079; †Applied Biotechnology Branch, Human Effectiveness Directorate, Air Force Research Laboratory, Wright-Patterson Air Force Base, Ohio 45433; and ‡NanoComposix, Inc., San Diego, California 92111

[1]To whom correspondence should be addressed at Neurochemistry Laboratory, Division of Neurotoxicology, HFT-132, National Center for Toxicological Research/Food and Drug Administration, 3900 NCTR Road, Jefferson, AR 72079. Fax: (870) 543-7745. E-mail: syed.ali@fda.hhs.gov.

Received May 17, 2010; accepted August 7, 2010

The current report examines the interactions of silver nano particles (Ag-NPs) with the cerebral microvasculature to identify the involvement of proinflammatory mediators that can increase blood-brain barrier (BBB) permeability. Primary rat brain microvessel endothelial cells (rBMEC) were isolated from adult Sprague-Dawley rats for an *in vitro* BBB model. The Ag-NPs were characterized by transmission electron microscopy (TEM), dynamic light scattering, and laser Doppler velocimetry. The cellular accumulation, cytotoxicity (6.25–50 μg/cm^3) and potential proinflammatory mediators (interleukin [IL]-1β, IL-2, tumor necrosis factor [TNF] α, and prostaglandin E_2 [PGE_2]) of Ag-NPs (25, 40, or 80 nm) were determined spectrophotometrically, cell proliferation assay (2,3-bis[2-methoxy-4-nitro-5-sulfophenyl]-2H-tetrazolium-5-carboxanilide) and ELISA. The results show Ag-NPs–induced cytotoxic responses at lower concentrations for 25 and 40 nm when compared with 80-nm Ag-NPs. The proinflammatory responses in this study demonstrate both Ag-NPs size and time-dependent profiles, with IL-1B preceding both TNF and PGE_2 for 25 nm. However, larger Ag-NPs (40 and 80 nm) induced significant TNF responses at 4 and 8 h, with no observable PGE_2 response. The increased fluorescein transport observed in this study clearly indicates size-dependent increases in BBB permeability correlated with the severity of immunotoxicity. Together, these data clearly demonstrate that larger Ag-NPs (80 nm) had significantly less effect on rBMEC, whereas the smaller particles induced significant effects on all the end points at lower concentrations and/or shorter times. Further, this study suggests that Ag-NPs may interact with the cerebral microvasculature producing a proinflammatory cascade, if left unchecked; these events may further induce brain inflammation and neurotoxicity.

Key Words: **blood-brain barrier; neuroinflamation; silver nanoparticles; rat brain microvessel endothelial cells; neurotoxicity.**

Silver nanoparticles (Ag-NPs) are small (1–100 nm in size) metallic colloidal particles widely used in the engineering, manufacturing, and biomedicine. Currently, there a several consumer products that contain various silver nanoparticles for their antimicrobial properties. The impact on human health of these metallic colloidal nanoparticles has not been adequately evaluated. With respect to blood-brain barrier (BBB) function and neurotoxicity, studies have shown that silver nanoparticles introduced into the systemic blood supply can induce BBB dysfunction, astrocyte swelling, in addition to, causing neuronal degeneration (Sharma *et al*., 2009a, 2009b). However, a comprehensive understanding of how Ag-NPs induce BBB dysfunction and neurotoxicity at the cellular level from the systemic blood supply remains largely unknown. Therefore, the current report examines the interactions of various sized commercially available silver nanoparticles (Ag-NPs) (25, 40, and 80 nm) with the cerebral microvasculature to identify the involvement of proinflammatory mediators in the increased BBB permeability associated with Ag-NPs exposure via the systemic blood supply. To our knowledge, this report is the first to evaluate the molecular mechanisms and integrity of the BBB *in vitro* following exposure to Ag-NPs. The primary brain microvessel endothelial cells (BMEC) isolated from cerebral cortices provide a well-suited *in vitro* model to evaluate BBB molecular mechanisms and transport characteristics in a high-throughput manner (Audus and Borchardt, 1987; Franke *et al*., 1999, 2000; Weber et al. 1993). These *in vitro* model systems grow polarized cell monolayers representative of the BBB (Audus and Borchardt, 1987; Franke *et al*., 1999, 2000; Weber *et al*., 1993). Since the discovery of the BBB by Ehrlich in 1885, the BBB is now considered a highly specialized organ tissue that serves as a barrier regulating the entry of molecules and substances into the brain from the systemic blood supply.

However, immunological, chemical, or physical insult can cause a dysfunction of the BBB, resulting in increased permeability of the brain capillaries and allowing the entry of substances into the brain from the blood that would normally be excluded. To date, several serious cerebral inflammatory disorders are associated with a compromised BBB (Langford and Masliah, 2001; Sharief *et al*., 1992, 1993). The severity of BBB disruptions associated with these cerebral inflammatory diseases is directly proportionate to the severity of the clinical condition (Beaumont *et al*., 2002; Langford, 2001).

Inflammation is mediated by a concerted production of inflammatory mediators, such as cytokines (interleukin-1 beta [IL-1B], tumor necrosis factor alpha [TNFα]), chemokines, adhesion molecules, and enzymes (cyclooxygenase, nitric oxide synthase, and matrix metalloproteinase [MMP]) that regulate the infiltration of peripheral leukocytes into the brain tissues and contribute to brain damage (Barone and Feuerstein, 1999; del Zoppo and Hallenbeck, 2000; del Zoppo *et al*., 2000). One of the major targets for these inflammatory mediators is the cerebral microvasculature, and isolated primary cerebral microvessel endothelial cells have been well correlated with event cascades that release proinflammatory cytokines *in vitro* (Claudio *et al*., 1994; Deli *et al*., 1995; de Vries *et al*., 1996) and *in vivo* (Abraham *et al*., 1996; Buttini *et al*., 1996; Claudio *et al*., 1994; Deli *et al*., 1995; de Vries *et al*. 1996; Saito *et al*., 1996). TNF or IL-1B have also been shown to increase brain microvascular permeability (Abraham *et al*., 1996; Didier *et al*., 2003; Deli *et al*., 1995; de Vries *et al*., 1996; Fiala *et al*., 1997; Mark and Miller, 1999; Mark *et al*., 2001; Mayhan, 2002; Saija *et al*., 1995; Tsao *et al*., 2001). Previous studies have linked the effects of TNF on the cerebral vasculature with several second messengers including vasodilators like prostaglandin E_2 (PGE_2) and nitric oxide (Bove *et al*., 2001; Horton, 2003; Mark *et al*., 2001; Vadeboncoeur *et al*., 2003). These well-correlated event cascades provide a sound foundation to utilize an *in vitro* model of the BBB to examine the proinflammatory mechanisms involved in the increased brain permeability following exposure to Ag-NPs. This approach will exclude other confounding variables associated with immunoresponsive hematopoietic cells.

In the current study, primary cultured rat brain microvessel endothelial cells (rBMEC) were used as an *in vitro* model system to examine the cellular accumulation, the changes in proinflammatory mediators, along with the changes in monolayer morphology and permeability following exposure to Ag-NPs similar to systemic blood supply route of exposure. The current report demonstrates that Ag-NPs accumulate with rBMEC in a size-dependent manner. The cellular association of Ag-NPs produces significant cytotoxicity and induces the release of cytokines and other inflammatory mediators from the rBMEC cell monolayers. The specific changes in the proinflammatory mediators correlate to morphological changes and increased permeability in rBMEC. The interactions of Ag-NPs at the apical surface (blood side) of the cerebral microvasculature produce several time-dependent proinflammatory mediators that may be the initial responses in BBB dysfunction, astrocyte swelling, and neuronal degeneration associated with Ag-NPs following systemic blood supply exposure previously reported (Sharma *et al*., 2009a, 2009b).

MATERIALS AND METHODS

Nanoparticle characterization using transmission electron microscopy. Transmission electron microscopy (TEM) characterization was performed to obtain the primary particle size and morphology of nanoparticles using a Hitachi H-7600 tungsten-tip instrument at an accelerating voltage of 100 kV. Nanoparticles were examined after dilution of nanoparticle stock solutions to 100 $\mu g/cm^3$ suspensions in water and subsequent deposition of 5 µl onto formvar-carbon–coated copper TEM grids which were then dried. Image J software was then used to measure the nanoparticles. The mean and SD of particle sizes was calculated from measuring over 100 nanoparticles in random fields of view in addition to the images showing the general morphology of the nanoparticles as previously described (Murdock *et al*., 2008).

Nanoparticle characterization using dynamic light scattering and laser Doppler velocimetry. Dynamic light scattering (DLS) and laser Doppler velocimetry (LDV), for characterization of size and zeta potential of the nanoparticles in solution, respectively, were performed on a Malvern Instruments Zetasizer Nano-ZS instrument. Samples were examined after dilution of nanoparticle stock solutions to 100 $\mu g/cm^3$ suspensions in DI water and rBMEC complete media, vortexed to provide a homogeneous solution, and then 1 cm^3 was transferred to a Malvern Clear Zeta Potential cell for DLS and LDV measurements (water dispersion) or to a 1-cm^2 plastic cuvette for DLS (media dispersion) as previously described (Murdock *et al*., 2008).

Cell isolation and culturing. rBMEC were isolated from a modified method as previously described (Audus and Borchardt, 1987). Briefly, the meninges were removed from the brain tissue of fresh rat (adult, Sprague-Dawley) cerebral cortices and mechanically homogenized through a 100-µm mesh screen. Dispase II enzyme (5 mg/cm^3) reconstituted in minimal essential medium (MEM) isolation media (MEM [1M], HEPES [50mM], polymyxin B [50 $\mu g/cm^3$], gentamicin [50 $\mu g/cm^3$], and amphotericin B [2.5 $\mu g/cm^3$] at pH 7.4) was added to the freshly homogenized cerebral cortical tissue (10 mg/g brain tissue), and MEM isolation media at pH 9.0 was added (equal wt/wt of brain tissue). The mixture was placed in an incubated shaker for 1 h (37°C, 150 revolutions per minute [rpm]). Following this incubation, the supernatant was removed by centrifugation (10 min at 1570 × g). The crude capillaries were isolated by resuspending the cerebral cortical tissue in a solution (13% [wt/vol] dextran supplemented with MEM [1M], HEPES [50mM], gentamicin [40 $\mu g/cm^3$], polymyxin B [50 $\mu g/cm^3$], and amphotericin B [2.5 $\mu g/cm^3$]) followed by centrifugation (10 min at 9170 × g). The crude capillary pellet was collected and resuspended in a collagenase/dispase (5 mg/cm^3) solution at a final concentration of 0.1% (vol/wt) and placed in an incubated shaker (37°C, 150 rpm) for 1 h. During this time, a percoll gradient (50% final concentration, supplemented with MEM [1M], HEPES [50mM], gentamicin [40 $\mu g/cm^3$], polymyxin B [50 $\mu g/cm^3$], and amphotericin B [2.5 $\mu g/cm^3$]) was set up by centrifugation (60 min at 39,200 × g). The digested capillaries were centrifuged (10 min, 1700 × g) to remove the enzymatic treatment and resuspended in isolation media and pipetted into the percoll gradient tubes. The rBMEC cells were then separated by centrifugation (10 min at 1700 × g). The freshly isolated rBMEC were extracted from the percoll gradient (3 cc syringe), pelleted, and resuspended in complete media (45% [vol/vol] MEM, 45% [vol/vol] Ham's F-12 nutrient mix, supplemented with 10mM HEPES, 13mM sodium bicarbonate, 50 $\mu g/cm^3$ gentamicin, 20% [vol/vol] FBS, 2.5 $\mu g/cm^3$

amphotericin B, and 100 μg/cm^3 sodium heparin). The rBMEC were plated, seeding density of approximately 50,000 cells/cm^2, on collagen-coated, fibronectin-treated culture plates, and incubated in a humidified incubator (37°C with 5% [vol/vol] CO_2). The cells were used after reaching confluence, typically 8–14 days.

The cellular association and accumulation of silver nanoparticles in rBMEC. The extent of cellular accumulation for the various sized Ag-NPs in rBMEC was evaluated spectrophotometrically (microplate reader at 450 nm). In these studies, the cell monolayers were seeded in standard six-well tissue culture plates (seeding density of 500,000 cells/cm^2) and cultured until confluence in a humidified chamber at 37°C supplemented with complete growth media as described above. Confluent cell monolayers were treated with a single bolus suspension of the various sized Ag-NPs for various times (30–60 min) (final dose 10.4 μg/cm^2) (concentration 50 μg/cm^3, volume of 2 cm^3, and surface area of 9.6 cm^2). The cell monolayers were then washed three times with ice-cold PBS and lysed (1% Triton-X [vol/vol] with protease inhibitor cocktail). The cell monolayer lysates (100 μl) and extracellular media (100 μl) were evaluated for the accumulated fraction of Ag-NPs. The fraction accumulated was normalized by total cellular protein by the BCA method as previously described (Bachmeier *et al*., 2004, 2006; Trickler *et al*., 2008, Trickler *et al*.). The cellular data are presented as a percent of Ag-NPs accumulated per milligram total cellular protein (mean ± SD, $n = 3$).

The cytotoxicity profile of various sized silver nanoparticles. The cell viability of rBMEC following exposure to various sized Ag-NPs was determined by measuring the mitochondrial dependent reduction of colorless 2,3-bis[2-methoxy-4-nitro-5-sulfophenyl]-2H-tetrazolium-5-carboxanilide (XTT) to a blue-colored formazan crystals. Briefly, the cells were seeded in a 96-well cell culture plate at a density of 5000 cells/well in 100 μl of growth media and cultured until confluence in complete growth media. The cells were treated with various sized Ag-NPs (25, 40, and 80 nm) for 24 h (dose range: 1.95–15.63 μg/cm^2) (6.25–50 μg/cm^3, volume of 0.1 cm^3, and surface area of 0.32 cm^2), then gently washed three times with ice-cold PBS (pH 7.4), and supplied with fresh growth media (150 μl/well) containing fresh XTT reagent (300 μg/cm^3) and phenazine methosulfate (37.5μM final concentration) and further incubated for 2 h at ambient temperature. The absorbance was determined using a microplate reader at 450 nm with reference wavelength of 650 nm. The absorbance data were analyzed and corrected for interference by subtracting absorbance of the Ag-NPs and cells prior to the addition of XTT reagents. The data are presented as percent survival of control monolayers receiving media alone (mean ± SD, $n = 3$).

rBMEC monolayer morphology following exposure to various silver nanoparticles. The rBMEC monolayer morphology was evaluated following exposure to various sized Ag-NPs was evaluated microscopically. In these studies, the cell monolayers were cultured in standard six-well tissue culture plates at a seeding density of 500,000 cells/cm^2 and cultured until confluence in a humidified chamber at 37°C supplemented with complete growth media as described above. Confluent cell monolayers were treated with the various sized Ag-NPs for 24 h (final dose 5.2 μg/cm^2) (concentration 25 μg/cm^3, volume of 2 cm^3, and surface area of 9.6 cm^2). The cell monolayers were viewed using a Nikon Eclipse TiE inverted microscope system with Fi1-L2 camera, differential interference contrast, and Phase contrast (utilizes NIS-Elements Advanced Research software version 3.1). The micrographs are representative of three monolayers, and the alterations in cell morphology and monolayer integrity were noted.

Prostaglandin E_2 release in rBMEC. The release of PGE_2 from the rBMEC monolayers was determined using a PGE_2-specific ELISA kit (R&D Systems, Cambridge, MA). Cross-reactivity for other prostaglandins was 70, 16.3, 1.4, and 0.7% for PGE_1, PGE_3, $PGF_{1\alpha}$, and $PGF_{2\alpha}$ respectively. Confluent rBMEC monolayers grown on six-well culture plates were placed in fresh complete culture media (2 cm^3) 24 h prior to silver nanoparticle exposure. After 24 h, the cell monolayers were treated with the various sized Ag-NPs (final dose 10.4 μg/cm^2) (concentration 50 μg/cm^3, volume of 2 cm^3, and surface area of 9.6 cm^2). Media was sampled (50 μl) at various time points following exposure to Ag-NPs (0–8 h) for use in the PGE_2 ELISA. The amount of PGE_2 released into the culture media was standardized based on the protein content of the cell monolayers, as determined by BCA protein assay. The results are presented as the average amount of PGE_2 per milligram protein (mean ± SEM, $n = 3$).

Cytokine release in rBMEC. The release of TNFα, IL-1β, and IL-2 were determined in rBMEC monolayers in response to silver nanoparticle exposure. The cytokines were measured using commercially available ELISA kits (R&D Systems). Cross-reactivity for TNFα and IL-1β from other species and other cytokines was not observed, and the limit of detection was less than 6 and 15 pg/cm^3, respectively. Confluent rBMEC monolayers grown on six-well culture plates were placed in fresh complete culture media (2 cm^3) 24 h prior to the experiment. After 24 h, the cell monolayers were treated with the various sized Ag-NPs (final dose 10.4 μg/cm^2) (concentration 50 μg/cm^3, volume of 2 cm^3, and surface area of 9.6 cm^2). Media was sampled (50 μl) at various time points following Ag-NPs exposure (0–8 h) and processed as described in the ELISA protocol. Concentrations of TNFα, IL-1β, and IL-2 released into the culture media were corrected for the amount of cellular protein as determined by BCA protein assay. The results are presented as the average amount of cytokine per milligram protein (mean ± SEM, $n = 3$).

Silver nanoparticle exposure effects permeability in rBMEC. The effects of various sized Ag-NPs exposure on the permeability of primary rBMEC monolayers were determined as described previously (Mark and Miller, 1999; Mark *et al*., 2001; Trickler *et al*., 2005). Briefly, the freshly isolated rBMEC were plated in triplicates at a seeding density of 50,000 cells/cm^2 on collagen-coated, fibronectin-treated, polycarbonate membrane inserts, and cultured until confluence (12 mm; 3.0 μm pore size, Costar Transwell 12-well, Cambridge, MA). Complete culture media from confluent rBMEC monolayers was replaced 24 h prior to the start of the experiment. The various sized Ag-NPs were diluted in complete culture media and spiked into the apical chamber (final dose 10.1 μg/cm^2) (concentration 15 μg/cm^3, volume of 0.6 cm^3, and surface area of 1.12 cm^2), and incubated for 24 h in a humidified incubator supplemented with 5% CO_2 at 37°C. Following the 24-h exposure period, the treatment media was removed from both apical and basolateral sides and replaced with fresh assay II buffer with (apical) or without (basolateral) fluorescein (10μM). Samples (100 μl) were removed from the basolateral compartment at various time points (0–90 min) and replaced with fresh buffer. The concentration of fluorescein in the samples was determined using a Chameleon microplate spectrophotofluorometer (485-nm excitation and 530-nm emission wavelengths). Permeability was expressed as the percent flux of the fluorescein marker across the rBMEC monolayers over time (mean ± SD, $n = 3$). The apparent permeability coefficient was calculated as previously described using the following Equation 1 (Karlsson and Artursson, 1992

$$P_{app} = \frac{1}{AC_0} \cdot \frac{dQ}{dt}, \quad (1)$$

where, dQ/dt is the flux across the cell monolayers, A is the surface area of the membrane, and C_0 is the initial concentration of fluorescein.

Materials and statistics. The Ag-NPs were a gift from Nanocomposix (San Diego, CA). The formulation of the Ag-NPs is as follows: 25 nm (50 mg/ml) are polyvinylpyrrolidone (PVP) coated (PVP 40 kDa), the 40-nm Ag-NPs (9.2 mg/ml) are PVP coated (PVP 10 kDa), and 80 nm (49 mg/ml) PVP coated (PVP 40 kDa). ELISA kits for PGE_2, TNF, IL-1B, and IL-2 were purchased from R&D Systems. All remaining media, media supplements, and reagents were obtained from Sigma Chemical Company (St Louis, MO). Statistical analyses of the various treatment effects were determined using nonparametric Kruskal-Wallis ANOVA with Tukey multiple *post hoc* comparisons of means. For all studies, statistical significance was designated as $p < 0.05$, unless otherwise stated.

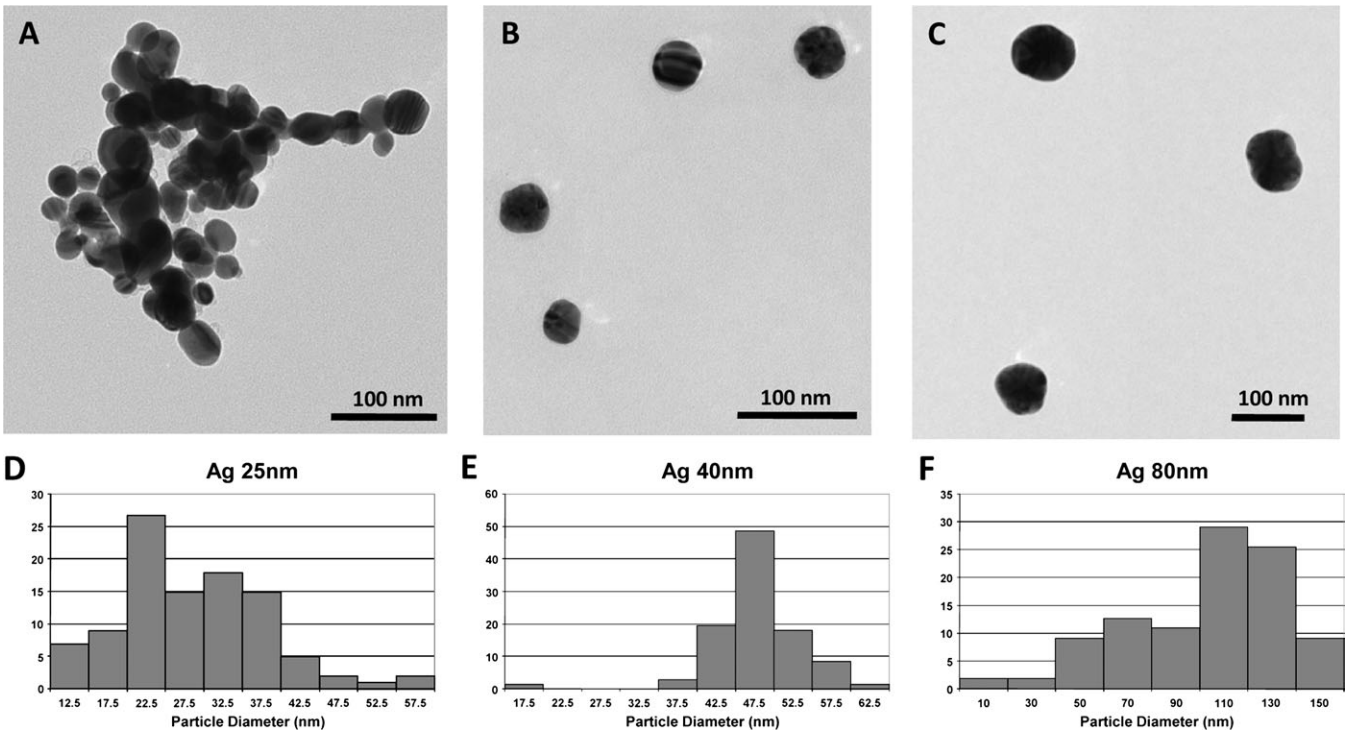

FIG. 1. TEM characterization of silver nanoparticles. Particles were spotted onto formvar-carbon–coated grids and dried prior to TEM imaging. Imaging was conducted in high-resolution mode at 100 kV. Particle size distributions were obtained by measuring using Image J with $n > 100$ for each sample. (A) Ag 25 nm imaged at 80 k× magnification. (B) Ag 40 nm imaged at 80 k× magnification. (C) Ag 80 nm imaged at 40 k× magnification. (D) Ag 25-nm size distribution histogram. (E) Ag 40-nm size distribution histogram. (F) Ag 40-nm size distribution histogram.

RESULTS

Nanoparticle Characterization Using TEM

TEM imaging of the Ag-NPs 25, 40, and 80 nm were performed to confirm primary particle size, obtain a size distribution, and observe the general morphology of the particles. In Figure 1A, the Ag-NPs 25 nm are shown with a generally spherical morphology. The size distribution of the Ag-NPs 25 nm (Fig. 1D) revealed some sample variability with respect to size (~75% falling within 20–40 nm in size), and the overall average differs slightly from the manufacturer's specifications at 28.3 ± 9.6 nm (Table 1). The Ag-NPs 40 nm (Fig. 1B) were very uniform in size and had mostly spherical morphology; however, a small percentage of the particles had a triangular morphology. Figure 1E shows the relative frequency of size measured with respect to the 40-nm Ag-NPs sample, with ~86% of the particles between 40 and 55 nm in size, and the overall average size was 47.5 ± 5.6 nm (Table 1). The 80-nm Ag-NPs (Fig. 1C) also display a spherical morphology; however, this sample showed the most variability in sizes present (Fig. 1F), with ~78% of the particles occurring in the 60- to 140-nm range. The overall average size of the 80-nm Ag-NPs sample was found to be 102.2 ± 32.8 nm (Table 1).

Nanoparticle Characterization Using DLS and LDV

The DLS and LDV results are shown in Table 1, where each particle was measured for size in solution and surface charge in

TABLE 1
Characterization Silver Nanoparticles Summary

	TEM	DLS		LDV	
Particle	Size distribution (nm)	*Z*-average diameter (nm)	PdI	Zeta potential ζ (mV)	Electrophoretic mobility U (μm·cm/[Vs])
Ag 25 nm	28.3 ± 9.6				
DI H_2O		106	0.379	−44.2	−3.46
rBMEC media		393	0.473	n/d	n/d
Ag 40 nm	47.5 ± 5.6				
DI H_2O		54.9	0.122	−46.0	−3.6
rBMEC media		73.9	0.191	n/d	n/d
Ag 80 nm	102.2 ± 32.8				
DI H_2O		177	0.048	−29.5	−2.32
rBMEC media		166	0.060	n/d	n/d

Note. TEM particle size distributions were obtained by measuring using Image J with $n > 100$ for each sample. For DLS and LDV studies, particle were dispersed in the respective solution, vortexed for homogeneity, and then placed in either a cuvette or a folded capillary tube for measurement. n/d, not determined.

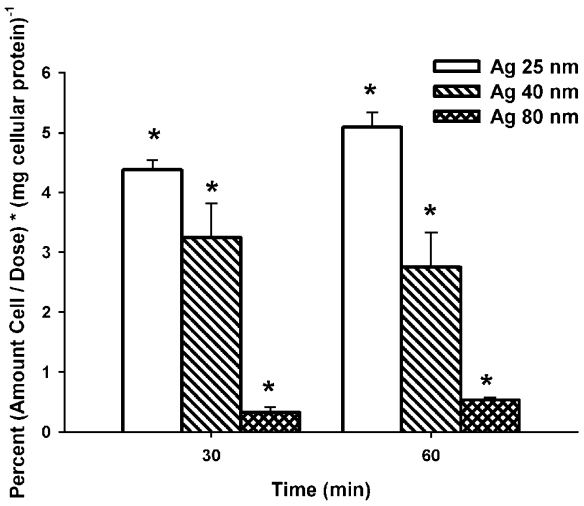

FIG. 2. The size-dependent accumulation of silver nanoparticles in rat brain microvessel endothelial cells. Triplicate cell monolayers were treated with various sized Ag-NPs (final dose 10.4 μg/cm^2) (concentration 50 μg/cm^3, volume of 2 cm^3, and surface area of 9.6 cm^2) (25 nm [open bars], 40 nm [diagonal bars], and 80 nm [crosshatch bars]). The data were determined by percentage of (amount in cell/dose) × (milligram cellular protein)$^{-1}$ and expressed as means ± SD, $n = 3$; ''*'' is considered statistically different when compared with time-matched groups $p < 0.05$.

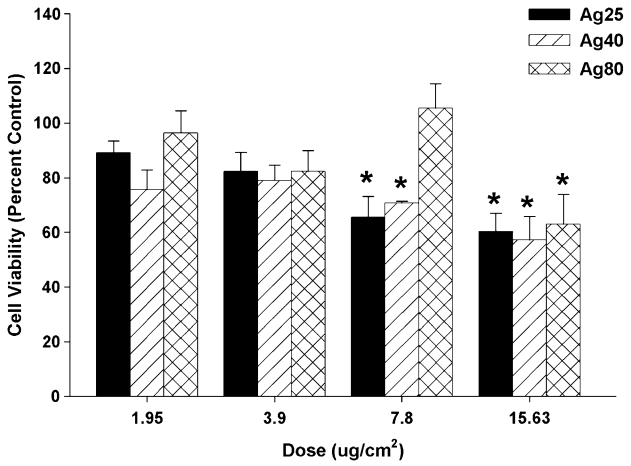

FIG. 3. The cytotoxicity profile of various sized silver nanoparticles. Triplicate cell monolayers were treated with various sized Ag-NPs (dose range 1.95–15.63 μg/cm^2) (6.25–50 μg/cm^3, volume of 0.1 cm^3, and surface area of 0.32 cm^2); (25 nm [closed black bars], 40 nm [diagonal bars], and 80 nm [crosshatched bars]). The data are expressed as means ± SD, $n = 3$; ''*'' is considered statistically significant when compared with time-matched control $p < 0.05$.

both DI H_2O and rBMEC complete media. The 25-nm Ag-NPs exhibited moderate aggregation in water, with a *Z*-average sizes of 106 nm; however, when dispersed in the rBMEC media, agglomeration increased by nearly fourfold to 393 nm (Table 1). The 40-nm Ag-NPs were found to have little to no aggregation in water at 54.9 nm, with only a slight average size increase to 73.9 nm when dispersed in media (Table 1). For the 80-nm Ag-NPs, only a slight difference was observed between aggregation in water and media at 177 and 166 nm, respectively (Table 1). However, an interesting pattern in the agglomeration was found for the 80-nm Ag-NPs. The agglomeration was found to be fairly uniform because of the PdI values being below 0.1, which means most of the aggregates formed were similar in size and could be caused by smaller particles collecting around some of the larger particles in the sample. The zeta potential values obtained for the 25-, 40-, and 80-nm Ag-NPs in water were all found to be negative at −44.2, −46.0, and −29.5 mV, respectively, which also indicate that they are stable in suspension (Table 1).

The Cellular Association and Accumulation of Silver Nanoparticles in Rat BMEC

The cellular association of the various sized Ag-NPs (25, 40, and 80 nm) was evaluated to determine the extent of adherence with primary rat BMEC (Fig. 2). There was a size-dependent accumulation observed for Ag-NPs in the rBMEC cells at both experimental times evaluated. At 30-min postexposure, the accumulation of 25 or 40 nm Ag-NPs were approximately 8.5- or 6-fold higher, respectively, when compared with 80-nm Ag-NPs. At 60-min postexposure, the accumulation of 25-nm Ag-NPs increased to approximately 10, whereas the 40-nm Ag-NPs remained sixfold when compared with 80-nm Ag-NPs. With the exception to the 40-nm Ag-NPs, there was an observed time-dependent accumulation increase for the 25- and 80-nm Ag-NPs.

The Cytotoxicity Profile of Various Sized Silver Nanoparticles

The cytotoxicity profile of the various sized Ag-NPs (25, 40, and 80 nm) was determined by the mitochondrial dependent conversion of XTT reagent in primary rat BMEC at 24 h postexposure (Fig. 3). The Ag-NPs showed significant decreased cell viability at the higher concentrations examined (25 and 50 μg/cm^3). Ag-NPs of 25- and 40-nm size showed significantly decreased cell viability at both 25 and 50 μg/cm^3. In contrast, Ag-NPs of 80-nm size only exhibited significant decreased cell viability at 50 μg/cm^3.

rBMEC Monolayer Morphology Following Exposure to Various Silver Nanoparticles

The morphology of rBMEC monolayers were evaluated microscopically after exposure to various sized Ag-NPs (Figs. 4a–d). When compared with control monolayers, the various sized Ag-NPs produced significant morphological changes in the rat BMEC (Figs. 4a–d). These morphological changes appear to be size dependent. Treatment with 25-nm Ag-NPs, the rat BMEC monolayers showed significantly more cellular damage with the appearance of large perforations in the monolayers (Fig. 4b) when compared with control monolayers. Treatment with 40- and 80-nm Ag-NPs also produced some cell morphology alterations; however, the perforations are observed to be significantly smaller and less frequent (Figs. 4c and 4d).

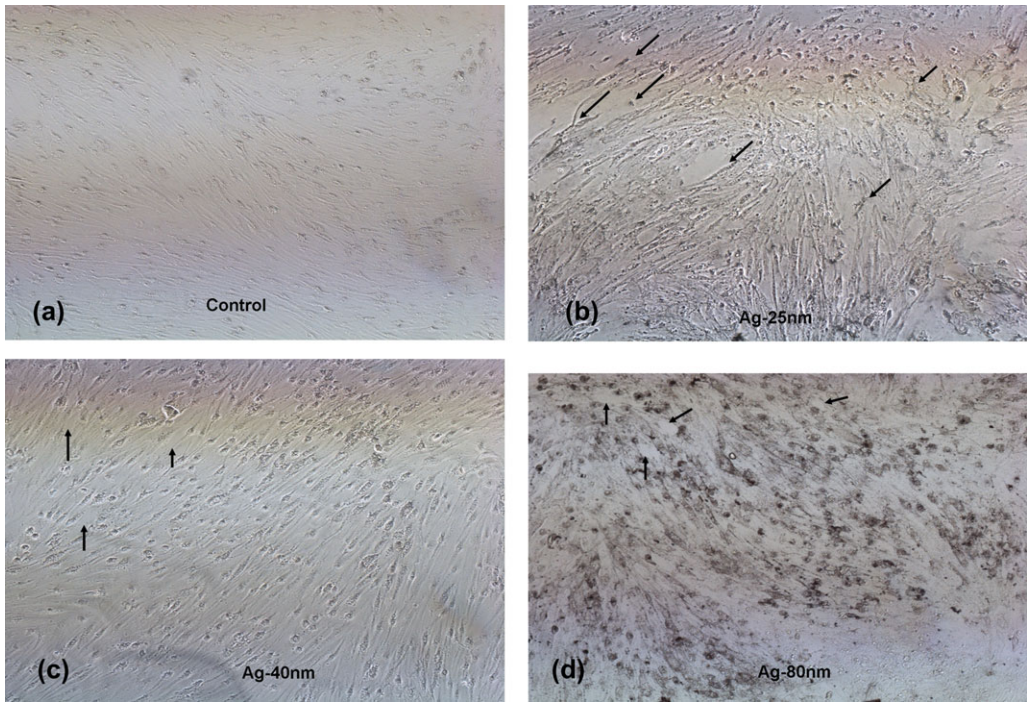

FIG. 4. rBMEC monolayer integrity following exposure to various silver nanoparticles. Cell monolayers were treated with various sized Ag-NPs for 24 h (final dose 5.2 μg/cm^2) (concentration 25 μg/cm^3, volume of 2 cm^3, and surface area of 9.6 cm^2); (a) media alone, (b) silver 25 nm, (c) silver 40 nm, and (d) silver 80 nm; ×10 magnification. The arrows indicate the presence of perforations in the rBMEC monolayers.

Prostaglandin E_2 Release in rBMEC

The release of PGE_2 from the rat BMEC monolayers was evaluated at various time intervals (0–8 h) following exposure to various sized Ag-NPs (25, 40, and 80 nm) (Fig. 5). The exposure of 25-nm Ag-NPs produced significant increases (fourfold) in PGE_2 release at 4-h postexposure when compared with control monolayers. The fourfold increase was persistent at 8-h postexposure. In addition, lipopolysaccharide (LPS) (positive control) exposure produced significant increased (approximately fivefold) PGE_2 release at 2-h postexposure that persisted for the entire experimental period (8 h). The larger Ag-NPs (40 and 80 nm) had no observable effect on PGE_2 release from rBMEC.

Cytokine Release in Rat BMEC

The time release profile of TNFα, IL-1β, and IL-2 and were determined in rat BMEC monolayers in response to various sized Ag-NPs (Figs. 6 and 7). TNF was released from the rat BMEC following all treatments at 4-h postexposure (Fig. 6). With the exception of the 80-nm Ag-NPs, significant release of TNF (at least fourfold) was observed following exposure to 25- and 40-nm Ag-NPs and LPS at 4-h postexposure (Fig. 6). The amount of TNF released following 25-nm Ag-NPs was similar when compared with the positive control (LPS) (approximately sixfold) at 8 h. Furthermore, at 8-h postexposure to Ag-NPs, the amount of TNF released displays a size-dependent profile at approximately sixfold, fivefold, and threefold for 25-, 40-, and 80-nm Ag NPs, respectively. The release of IL-1β also showed a time-dependent profile following exposure to various sized Ag-NPs (Fig. 7). However, exposure to 25-nm Ag-NPs produced a significant release of IL-1β (approximately

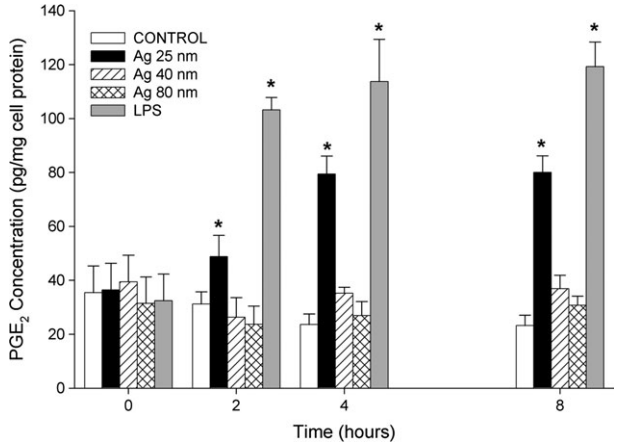

FIG. 5. Silver nanoparticle exposure affects PGE_2 release from the rBMEC. Triplicate cell monolayers were treated (50 μg/ml) with various size Ag-NPs (final dose 10.4 μg/cm^2) (concentration 50 μg/cm^3, volume of 2 cm^3, and surface area of 9.6 cm^2); control (open bars), silver 25 nm (closed black bars), silver 40 nm (diagonal bars), silver 80 nm (crosshatch bars), and LPS (closed light gray bar). The data are expressed as means ± SEM, $n = 3$; ''*'' is considered statistically significant when compared with time-matched control $p < 0.05$.

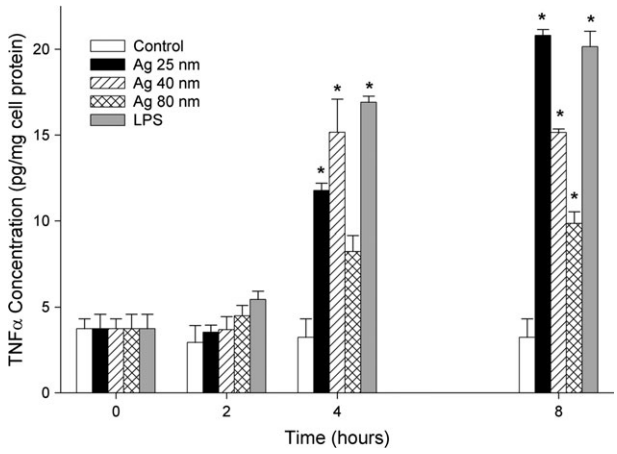

FIG. 6. Silver nanoparticle exposure affects TNFα release from the rBMEC. Triplicate cell monolayers were treated with various sized Ag-NPs (final dose 10.4 μg/cm^2) (concentration 50 μg/cm^3, volume of 2 cm^3, and surface area of 9.6 cm^2); control (open bars), silver 25 nm (closed black bars), silver 40 nm (diagonal bars), silver 80 nm (crosshatch bars), and LPS (closed light gray bar). The data are expressed as means ± SEM, $n = 3$; ''*'' is considered statistically significant when compared with time-matched control $p < 0.05$.

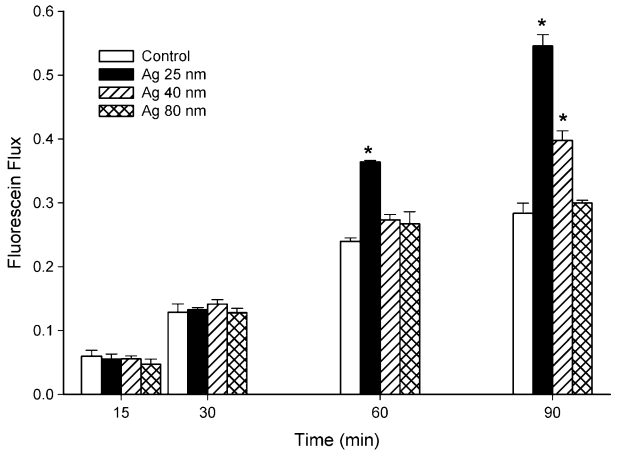

FIG. 8. Silver nanoparticle exposure affects permeability in rBMEC. Triplicate cell monolayers were treated with various sized Ag-NPs (final dose 10.1 μg/cm^2) (concentration 15 μg/cm^3, volume of 0.6 cm^3, and surface area of 1.12 cm^2); control (open bars), silver 25 nm (closed black bars), silver 40 nm (diagonal bars), and silver 80 nm (crosshatch bars). The data are expressed as means ± SD, $n = 3$; ''*'' is considered statistically significant when compared with time-matched control $p < 0.05$.

fourfold) as early as 2 h when compared with control. At 4-h postexposure, significant increases of IL-1β (approximately fivefold) were observed for 25- and 40-nm Ag-NPs, and these increases were similar to LPS. At 8-h postexposure, significant increases in IL-1β release were only observed for 25-nm Ag-NPs and LPS (7-fold and 14-fold, respectively) when compared with control monolayers. The release of IL-2 from the rat BMEC over the experimental period examined was unremarkable (data not shown).

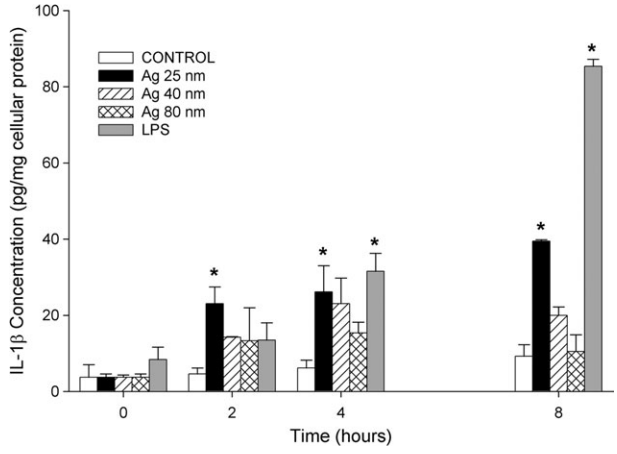

FIG. 7. Silver nanoparticle exposure affects IL-1β release from the rBMEC. Triplicate cell monolayers were treated with various size Ag-NPs (final dose 10.4 μg/cm^2) (concentration 50 μg/cm^3, volume of 2 cm^3, and surface area of 9.6 cm^2); control (open bars), silver 25 nm (closed black bars), silver 40 nm (diagonal bars), silver 80 nm (crosshatch bars), and LPS (closed light gray bar). The data are expressed as means ± SEM, $n = 3$; ''*'' is considered statistically significant when compared with time-matched control $p < 0.05$.

Silver Nanoparticle Exposure Effects Permeability in rBMEC

The permeability effects were determined by evaluating the transport of fluorescein across rBMEC cell monolayers following apical (blood side) exposure to various sized Ag-NPs (Fig. 8); 25-nm Ag-NPs significantly increased the permeability of fluorescein (from the apical compartment to the basolateral compartment) across the rBMEC monolayers over the 90-min experimental time frame. The magnitude of the effect was nearly twofold. However, 40-nm Ag-NPs only produced significant increased permeability at the 90-min time point. The magnitude of the effect was approximately 1.3-fold. The change in permeability for rBMEC monolayers exposed to 80-nm Ag-NPs was unremarkable when compared with control monolayers. To further evaluate the changes in permeability following exposure to Ag-NPs, the apparent

TABLE 2
Apparent Permeability Changes Following Silver Nanoparticle Exposure

Treatment groups	Apparent permeability coefficient (1×10^{-6} cm/s)	Apparent permeability coefficient ratio (treatment/control)
Control	1.71 ± 0.060	1.00 ± 0.035
Ag 25 nm	3.43 ± 0.022*	1.88 ± 0.012*
Ag 40 nm	2.41 ± 0.006*	1.32 ± 0.004*
Ag 80 nm	1.93 ± 0.100	1.06 ± 0.055

Note. Calculated by: $P_{app} = \frac{1}{AC_0} \cdot \frac{dQ}{dt}$, where dQ/dt is the flux across the cell monolayers, A is the surface area of the membrane, and C_0 is the initial concentration of fluorescein. The data are presented as mean ± SD.

*Considered statistically different from control monolayers $p < 0.05$, $n = 3$.

permeability coefficients were determined (Table 2). The apparent permeability coefficients rank orders clearly demonstrate size-dependent permeability effects following exposure to Ag-NPs, with Ag-25 > Ag-40 > Ag-80 ≈ Control.

DISCUSSION

Currently, there are several consumer products that contain various silver nanoparticles for their antimicrobial properties. The impact on human health of these metallic colloidal nanoparticles has not been adequately evaluated. With respect to BBB function and neurotoxicity, the reports are limited. These limited studies have shown that silver nanoparticles introduced into the systemic blood supply can induce BBB dysfunction, astrocyte swelling, in addition to, causing neuronal degeneration *in vivo* (Sharma *et al.* 2009a, 2009b; Tang *et al.*, 2009). Tang and colleagues suggested the brain accumulation of silver ions by inductively coupled plasma mass spectrometry following subcutaneous injection (62.8 mg/kg) of silver nanoparticles but not silver microparticles (Tang *et al.*, 2009). Sharma *et al.* (2009a) demonstrated the leakage of Evan's blue dye and radioiodine following iv (30 mg/kg) or ip (50 mg/kg) administration of Ag-NPs. Sharma *et al.* (2009b) further suggested that the increased cerebral microvasculature permeability involves reactive oxygen species (ROS) generation because the increased permeability was attenuated by nanowire-antioxidant therapy following chronic exposure of Ag-NPs *in vivo* (Sharma *et al.*, 2009b). Although increased BBB permeability has been shown, little is known about the responses at the cellular level following Ag-NPs exposure. Therefore, the current report identifies a time-dependent proinflammatory response induced by Ag-NPs in a size-dependent manner at the cellular level in rBMEC, which is further evidenced by the increased BBB permeability of fluorescein. To our knowledge, this report is the first to evaluate the proinflammatory response and integrity of the BBB *in vitro* following exposure to Ag-NPs.

In the current study, the cellular association of Ag-NPs induces the increased release of various proinflammatory mediators (TNF, IL-1B, and PGE_2). The time-dependent profile and increased release of these particular proinflammatory mediators significantly correlate with the increased rBMEC permeability following exposure to Ag-NPs and further suggest that morphological changes in rBMEC monolayer integrity are associated with increased permeability. With respect to the cerebral microvasculature, previous studies have shown that immunological, chemical, or physical insult can cause a dysfunction of the BBB and well documented both *in vitro* and *in vivo* to include proinflammatory mediators like TNF, IL-1B, and PGE_2 (Abraham *et al.*, 1996; Barone and Feuerstein, 1999; Boje, 2001; Buttini et al. 1996; Caserta *et al.*, 1998, Dallasta *et al.*, 1999, de Vries *et al.*, 1996; del Zoppo *et al.*, 2000; Huber et al. 2001; Mark et al. 2001; Mayhan 2002; Perry *et al.*, 1997; Ponnampalam and Mayberg, 2004; Sharief *et al.*, 1992; Ujiie *et al.*, 2003; Wahl and Schilling, 1993; Webb and Muir, 2000). Further, the release of cytokines following cerebral microvasculature damage has been linked to oxidative free radical generation and growth factors (Calingasan *et al.*, 2000; Duchini, 1996; Ergenekon *et al.*, 2004; Fiala *et al.*, 1997; Hartung et al. 1992). The generation of ROS have been shown to be associated with toxicity following Ag-NPs exposure both *in vitro* and *in vivo* (Rahman *et al.*, 2009; Rosas-Hernandez *et al.*, 2009; Wang *et al.*, 2009). TNF or IL-1B have both been shown to increase brain microvascular permeability and linked with several second messengers including vasodilators like PGE_2 and nitric oxide both *in vitro* (Didier *et al.*, 2003; Deli *et al.*, 1995; de Vries *et al.*, 1996; Fiala *et al.*, 1997; Mark and Miller, 1999; Mark *et al.*, 2001; Trickler *et al.*, 2005) and *in vivo* (Abraham *et al.*, 1996; Mayhan, 2002; Saija *et al.*, 1995; Tsao *et al.*, 2001; Trickler *et al.*, 2005).

With respect to the responses in the cerebral microvasculature that have been shown to induce alterations in BBB integrity discussed above, there are several lines of evidence supporting the results in this report. First, the current studies clearly indicate that Ag-NPs accumulate and interact with the cerebral microvasculature in this *in vitro* model of the BBB. To our knowledge, this is the first report to utilize ultraviolet-visible spectroscopy as a rapid method to quantitatively evaluate the accumulation of Ag-NPs in biological samples. Although the magnitude of the fraction accumulated with the cerebral microvasculature cells observed in the present study was below 6% of the total dose normalized by total cellular protein (Fig. 2), the percentage accumulated was depended on the size of Ag-NPs and sufficient to cause cytotoxicity in rBMEC at concentrations of 7.8 $\mu g/cm^2$ and above (Fig. 2). Similar *in vitro* results have been reported elsewhere in other cell types (Carlson *et al.*, 2008; Hussain *et al.*, 2006; Mahmood *et al.*, 2010). Carlson *et al.* (2008) demonstrated that Ag-NPs exposure produced cells with morphologically abnormal size and adherence characteristics with significant uptake of Ag-NPs at high doses after 24 h in alveolar macrophages. In addition, cellular viability significantly decreased with increasing dose
(10–75 $\mu g/cm^3$) of Ag-NPs (15 and 30 nm) following 24 h of exposure. Furthermore, these studies demonstrated 24 h of exposure to Ag-NPs (15 nm); significant inflammatory responses were observed by the release of TNF, MIP-2, and IL-1B from alveolar macrophages (Carlson *et al.*, 2008). Mahmood *et al.* (2010) further demonstrated that at various concentrations Ag-NPs accumulated in a relatively short time in two cell lines (MLO-Y4 osteocytic cells and HeLa cervical cancer cells) and exposure significantly affected the size and shape of the cells for both cell types. Microscopic studies by Hussain *et al.* (2006) showed that nanoparticles and agglomerates were effectively internalized by PC-12 cells producing cellular shrinkage and irregular membrane borders. In addition, these studies showed that Ag-NPs produced significantly more

cytotoxicity than similar dose of manganese nanoparticles (Hussain *et al*., 2006).

With respect to cellular morphological changes, the current study also clearly demonstrates alterations in cellular morphology following exposure to Ag-NPs in rBMEC. The interactions of the Ag-NPs with rBMEC induce cellular damage in the observed monolayers with the appearance of perforations in the monolayers. The observed perforations appear to be dependent on the size of Ag-NPs (Figs. 4b–d) when compared with control (Fig. 4a). The size-dependent morphology changes in the rBMEC monolayers following the exposure of Ag-NPs were further evidenced with smaller Ag-NPs significantly increasing the fluorescein permeability compared with monolayers treated with larger Ag-NPs and control monolayers (Fig. 8 and Table 2). Furthermore, the size-dependent permeability changes associated with the exposure to Ag-NPs also correlate well with the release patterns of proinflammatory mediators in this report (Figs. 5–7). Together, the release time profiles for PGE_2, TNF, and IL-1B clearly show that the response for larger Ag-NPs (40 and 80 nm) was significantly diminished when compared with significantly more profound proinflammatory response observed with smaller Ag-NPs (25 nm).

In contrast with the results reported in this study, Sheikpranbabu *et al*. (2009) reported that Ag-NPs (40–50 nm) inhibit vascular endothelial growth factor (VEGF) and IL-1B–induced vascular permeability and cellular proliferation in porcine retinal endothelial cells *via* Src-dependent pathway (Sheikpranbabu *et al*., 2009). This may illustrate the significance of the methodologies used, species differences, or the tissue origin of the cells. However, significant methodology differences in exposure time maybe the contributing factor contrasting these studies (6 h compared with 24 h). Indeed, Gurunathan *et al*. (2009) and Kalishwarala *et al*. clearly demonstrate that Ag-NPs are antiangiogenic inhibiting VEGF-induced cellular proliferation at 24 h of exposure. However, both these reports also show that Ag-NPs inhibit the cell survival pathway phosphatidylinositol 3-kinase (PI3K)/Akt, clear enhancement of caspase 3 activity, and evidence of induction of apoptosis after 24 h of exposure in bovine retinal endothelial cells (Gurunathan *et al*., 2009; Kalishwaralal *et al*., 2009). Therefore, it appears that the time of exposure is of considerable importance and further investigation maybe warranted. However, species differences and tissue origin of the cells should not be overlooked.

Together, the data in the current report provide compelling evidence that systemic exposure of Ag-NPs can result in cerebral microvascular damage and dysfunction dependent on Ag-NPs size, with smaller Ag-NPs producing stronger inflammatory responses correlated with increased cerebral microvascular permeability, whereas the effects produced by the larger Ag-NPs were much less profound. These inflammatory-mediated increases in cerebral microvascular permeability allow the entry of molecules and substances into the brain tissues that are normally sequestered in the systemic blood supply and may contribute concomitantly to further brain inflammation and neurotoxicity.

ACKNOWLEDGMENTS

The contents of this manuscript do not necessarily reflect the views and policies of the U.S. Food & Drug Administration, and the mention of trade names or commercial products does not constitute endorsement or recommendation for use. This research was supported in part by an appointment to the Postgraduate Research Participation Program with the U. S. Air Force Research Laboratory at the National Center for Toxicological Research/FDA (Jefferson, AR) administered by the Oak Ridge Institute of Science and Education (Oak Ridge, TN) through an interagency agreement between U.S. Department of Energy, U. S. Air Force Research Laboratory/ Applied Biotechnology Branch, and the U. S. Food and Drug Administration.

REFERENCES

Abraham, C. S., Deli, M. A., Joo, F., Megyeri, P., and Torpier, G. (1996). Intracarotid tumor necrosis factor-alpha administration increases the blood-brain barrier permeability in cerebral cortex of the newborn pig: quantitative aspects of double-labelling studies and confocal laser scanning analysis. *Neurosci. Lett.* **208,** 85–88.

Audus, K. L., and Borchardt, R. T. (1987). Bovine brain microvessel endothelial cell monolayers as a model system for the blood-brain barrier. *Ann. N. Y. Acad. Sci.* **507,** 9–18.

Bachmeier, C. J., Trickler, W. J., and Miller, D. W. (2004). Drug efflux transport properties of 2',7'-bis(2-carboxyethyl)-5(6)-carboxyfluorescein acetoxymethyl ester (BCECF-AM) and its fluorescent free acid, BCECF. *J. Pharm. Sci.* **93,** 932–942.

Bachmeier, C. J., Trickler, W. J., and Miller, D. W. (2006). Comparison of drug efflux transport kinetics in various blood-brain barrier models. *Drug Metab. Dispos.* **34,** 998–1003.

Barone, F. C., and Feuerstein, G. Z. (1999). Inflammatory mediators and stroke: new opportunities for novel therapeutics. *J. Cereb. Blood Flow Metab.* **19,** 819–834.

Beaumont, A., Marmarou, A., Fatouros, P., and Corwin, F. (2002). Secondary insults worsen blood brain barrier dysfunction assessed by MRI in cerebral contusion. *Acta. Neurochir. Suppl.* **81,** 217–219.

Boje, K. M. (2001). *In vivo* measurement of blood-brain barrier permeability. *Curr. Protoc. Neurosci.* 7.19.1–7.19.39.

Bove, K., Neumann, P., Gertzberg, N., and Johnson, A. (2001). Role of ecNOS-derived NO in mediating TNF-induced endothelial barrier dysfunction. *Am. J. Physiol. Lung Cell. Mol. Physiol.* **280,** L914–L922.

Buttini, M., Limonta, S., and Boddeke, H. W. (1996). Peripheral administration of lipopolysaccharide induces activation of microglial cells in rat brain. *Neurochem. Int.* **29,** 25–35.

Calingasan, N. Y., Huang, P. L., Chun, H. S., Fabian, A., and Gibson, G. E. (2000). Vascular factors are critical in selective neuronal loss in an animal model of impaired oxidative metabolism. *J. Neuropathol. Exp. Neurol.* **59,** 207–217.

Carlson, C., Hussain, S. M., Schrand, A. M., Braydich-Stolle, L. K., Hess, K. L., Jones, R. L., and Schlager, J. J. (2008). Unique cellular interaction of silver

nanoparticles: size-dependent generation of reactive oxygen species. *J. Phys. Chem. B.* **112,** 13608–13619.

Caserta, M. T., Caccioppo, D., Lapin, G. D., Ragin, A., and Groothuis, D. R. (1998). Blood-brain barrier integrity in Alzheimer's disease patients and elderly control subjects. *J. Neuropsychiatry Clin. Neurosci.* **10,** 78–84.

Claudio, L., Martiney, J. A., and Brosnan, C. F. (1994). Ultrastructural studies of the blood-retina barrier after exposure to interleukin-1 beta or tumor necrosis factor-alpha. *Lab. Invest.* **70,** 850–861.

Dallasta, L. M., Pisarov, L. A., Esplen, J. E., Werley, J. V., Moses, A. V., Nelson, J. A., and Achim, C. L. (1999). Blood-brain barrier tight junction disruption in human immunodeficiency virus-1 encephalitis. *Am. J. Pathol.* **155,** 1915–1927.

de Vries, H. E., Blom-Roosemalen, M. C., van Oosten, M., de Boer, A. G., van Berkel, T. J., Breimer, D. D., and Kuiper, J. (1996). The influence of cytokines on the integrity of the blood-brain barrier in vitro. *J. Neuroimmunol.* **64,** 37–43.

del Zoppo, G., Ginis, I., Hallenbeck, J. M., Iadecola, C., Wang, X., and Feuerstein, G. Z. (2000). Inflammation and stroke: putative role for cytokines, adhesion molecules and iNOS in brain response to ischemia. *Brain Pathol.* **10,** 95–112.

del Zoppo, G. J., and Hallenbeck, J. M. (2000). Advances in the vascular pathophysiology of ischemic stroke. *Thromb. Res.* **98,** 73–81.

Deli, M. A., Descamps, L., Dehouck, M. P., Cecchelli, R., Joo, F., Abraham, C. S., and Torpier, G. (1995). Exposure of tumor necrosis factor-alpha to luminal membrane of bovine brain capillary endothelial cells cocultured with astrocytes induces a delayed increase of permeability and cytoplasmic stress fiber formation of actin. *J. Neurosci. Res.* **41,** 717–726.

Didier, N., Romero, I. A., Creminon, C., Wijkhuisen, A., Grassi, J., and Mabondzo, A. (2003). Secretion of interleukin-1beta by astrocytes mediates endothelin-1 and tumour necrosis factor-alpha effects on human brain microvascular endothelial cell permeability. *J. Neurochem.* **86,** 246–254.

Duchini, A. (1996). The role of central nervous system endothelial cell activation in the pathogenesis of hepatic encephalopathy. *Med. Hypotheses.* **46,** 239–244.

Ergenekon, E., Gucuyener, K., Erbas, D., Aral, S., Koc, E., and Atalay, Y. (2004). Cerebrospinal fluid and serum vascular endothelial growth factor and nitric oxide levels in newborns with hypoxic ischemic encephalopathy. *Brain Dev.* **26,** 283–286.

Fiala, M., Looney, D. J., Stins, M., Way, D. D., Zhang, L., Gan, X., Chiappelli, F., Schweitzer, E. S., Shapshak, P., Weinand, M., *et al.* (1997). TNF-alpha opens a paracellular route for HIV-1 invasion across the blood-brain barrier. *Mol. Med.* **3,** 553–564.

Franke, H., Galla, H., and Beuckmann, C. T. (2000). Primary cultures of brain microvessel endothelial cells: a valid and flexible model to study drug transport through the blood-brain barrier in vitro. *Brain Res. Brain Res. Protoc.* **5,** 248–256.

Franke, H., Galla, H. J., and Beuckmann, C. T. (1999). An improved low-permeability in vitro-model of the blood-brain barrier: transport studies on retinoids, sucrose, haloperidol, caffeine and mannitol. *Brain Res.* **818,** 65–71.

Gurunathan, S., Lee, K. J., Kalishwaralal, K., Sheikpranbabu, S., Vaidyanathan, R., and Eom, S. H. (2009). Antiangiogenic properties of silver nanoparticles. *Biomaterials* **30,** 6341–6350.

Hartung, H. P., Jung, S., Stoll, G., Zielasek, J., Schmidt, B., Archelos, J. J., and Toyka, K. V. (1992). Inflammatory mediators in demyelinating disorders of the CNS and PNS. *J. Neuroimmunol.* **40,** 197–210.

Horton, J. W. (2003). Free radicals and lipid peroxidation mediated injury in burn trauma: the role of antioxidant therapy. *Toxicology* **189,** 75–88.

Huber, J. D., Witt, K. A., Hom, S., Egleton, R. D., Mark, K. S., and Davis, T. P. (2001). Inflammatory pain alters blood-brain barrier permeability and tight junctional protein expression. *Am. J. Physiol. Heart Circ. Physiol.* **280,** H1241–H1248.

Hussain, S. M., Javorina, A. K., Schrand, A. M., Duhart, H. M., Ali, S. F., and Schlager, J. J. (2006). The interaction of manganese nanoparticles with PC-12 cells induces dopamine depletion. *Toxicol. Sci.* **92,** 456–463.

Kalishwaralal, K., Banumathi, E., Ram Kumar Pandian, S., Deepak, V., Muniyandi, J., Eom, S. H., and Gurunathan, S. (2009). Silver nanoparticles inhibit VEGF induced cell proliferation and migration in bovine retinal endothelial cells. *Colloids Surf. B Biointerfaces* **73,** 51–57.

Karlsson, J., and Artursson, P. (1992). A new diffusion chamber system for the determination of drug permeability coefficients across the human intestinal epithelium that are independent of the unstirred water layer. *Biochim. Biophys. Acta.* **1111,** 204–210.

Langford, C. A. (2001). Management of systemic vasculitis. *Best Pract. Res. Clin. Rheumatol.* **15,** 281–297.

Langford, D., and Masliah, E. (2001). Crosstalk between components of the blood brain barrier and cells of the CNS in microglial activation in AIDS. *Brain Pathol.* **11,** 306–312.

Mahmood, M., Casciano, D. A., Mocan, T., Iancu, C., Xu, Y., Mocan, L., Iancu, D. T., Dervishi, E., Li, Z., Abdalmuhsen, M., *et al.* (2010). Cytotoxicity and biological effects of functional nanomaterials delivered to various cell lines. *J. Appl. Toxicol.* **30,** 74–83.

Mark, K. S., and Miller, D. W. (1999). Increased permeability of primary cultured brain microvessel endothelial cell monolayers following TNF-alpha exposure. *Life Sci.* **64,** 1941–1953.

Mark, K. S., Trickler, W. J., and Miller, D. W. (2001). Tumor necrosis factor-alpha induces cyclooxygenase-2 expression and prostaglandin release in brain microvessel endothelial cells. *J. Pharmacol. Exp. Ther.* **297,** 1051–1058.

Mayhan, W. G. (2002). Cellular mechanisms by which tumor necrosis factor-alpha produces disruption of the blood-brain barrier. *Brain Res.* **927,** 144–152.

Murdock, R. C., Braydich-Stolle, L., Schrand, A. M., Schlager, J. J., and Hussain, S. M. (2008). Characterization of nanomaterial dispersion in solution prior to in vitro exposure using dynamic light scattering technique. *Toxicol. Sci.* **101,** 239–253.

Perry, V. H., Anthony, D. C., Bolton, S. J., and Brown, H. C. (1997). The blood-brain barrier and the inflammatory response. *Mol. Med. Today* **3,** 335–341.

Ponnampalam, S. N., and Mayberg, M. R. (2004). Mediators of blood-brain barrier disruption and potential therapeutic interventions for protection of the barrier following focal ischemia. *Clin. Neurosurg.* **51,** 112–119.

Rahman, M. F., Wang, J., Patterson, T. A., Saini, U. T., Robinson, B. L., Newport, G. D., Murdock, R. C., Schlager, J. J., Hussain, S. M., and Ali, S. F. (2009). Expression of genes related to oxidative stress in the mouse brain after exposure to silver-25 nanoparticles. *Toxicol. Lett.* **187,** 15–21.

Rosas-Hernandez, H., Jimenez-Badillo, S., Martinez-Cuevas, P. P., Gracia-Espino, E., Terrones, H., Terrones, M., Hussain, S. M., Ali, S. F., and Gonzalez, C. (2009). Effects of 45-nm silver nanoparticles on coronary endothelial cells and isolated rat aortic rings. *Toxicol. Lett.* **191,** 305–313.

Saija, A., Princi, P., Lanza, M., Scalese, M., Aramnejad, E., and De Sarro, A. (1995). Systemic cytokine administration can affect blood-brain barrier permeability in the rat. *Life Sci.* **56,** 775–784.

Saito, K., Suyama, K., Nishida, K., Sei, Y., and Basile, A. S. (1996). Early increases in TNF-alpha, IL-6 and IL-1 beta levels following transient cerebral ischemia in gerbil brain. *Neurosci. Lett.* **206,** 149–152.

Sharief, M. K., Ciardi, M., and Thompson, E. J. (1992). Blood-brain barrier damage in patients with bacterial meningitis: association with tumor necrosis factor-alpha but not interleukin-1 beta. *J. Infect. Dis.* **166,** 350–358.

Sharief, M. K., McLean, B., and Thompson, E. J. (1993). Elevated serum levels of tumor necrosis factor-alpha in Guillain-Barre syndrome. *Ann. Neurol.* **33,** 591–596.

Sharma, H. S., Ali, S. F., Hussain, S. M., Schlager, J. J., and Sharma, A. (2009a). Influence of engineered nanoparticles from metals on the blood-brain barrier permeability, cerebral blood flow, brain edema and neurotoxicity. An experimental study in the rat and mice using biochemical and morphological approaches. *J. Nanosci. Nanotechnol.* **9,** 5055–5072.

Sharma, H. S., Ali, S. F., Tian, Z. R., Hussain, S. M., Schlager, J. J., Sjoquist, P. O., Sharma, A., and Muresanu, D. F. (2009b). Chronic treatment with nanoparticles exacerbate hyperthermia induced blood-brain barrier breakdown, cognitive dysfunction and brain pathology in the rat. Neuroprotective effects of nanowired-antioxidant compound H-290/51. *J. Nanosci. Nanotechnol.* **9,** 5073–5090.

Sheikpranbabu, S., Kalishwaralal, K., Venkataraman, D., Eom, S. H., Park, J., and Gurunathan, S. (2009). Silver nanoparticles inhibit VEGF-and IL-1beta-induced vascular permeability via Src dependent pathway in porcine retinal endothelial cells. *J. Nanobiotechnol.* **7,** 8.

Tang, J., Xiong, L., Wang, S., Wang, J., Liu, L., Li, J., Yuan, F., and Xi, T. (2009). Distribution, translocation and accumulation of silver nanoparticles in rats. *J. Nanosci. Nanotechnol.* **9,** 4924–4932.

Trickler, W. J., Khurana, J., Nagvekar, A. A., and Dash, A. K. (2010). Chitosan and glyceryl monooleate nanostructures containing gemcitabine: potential delivery system for pancreatic cancer treatment. *AAPS PharmSciTech* **11,** 392–401.

Trickler, W. J., Mayhan, W. G., and Miller, D. W. (2005). Brain microvessel endothelial cell responses to tumor necrosis factor-alpha involve a nuclear factor kappa B (NF-kappaB) signal transduction pathway. *Brain Res.* **1048,** 24–31.

Trickler, W. J., Nagvekar, A. A., and Dash, A. K. (2008). A novel nanoparticle formulation for sustained paclitaxel delivery. *AAPS PharmSciTech.* **9,** 486–493.

Tsao, N., Hsu, H. P., Wu, C. M., Liu, C. C., and Lei, H. Y. (2001). Tumour necrosis factor-alpha causes an increase in blood-brain barrier permeability during sepsis. *J. Med. Microbiol.* **50,** 812–821.

Ujiie, M., Dickstein, D. L., Carlow, D. A., and Jefferies, W. A. (2003). Blood-brain barrier permeability precedes senile plaque formation in an Alzheimer disease model. *Microcirculation* **10,** 463–470.

Vadeboncoeur, N., Segura, M., Al-Numani, D., Vanier, G., and Gottschalk, M. (2003). Pro-inflammatory cytokine and chemokine release by human brain microvascular endothelial cells stimulated by Streptococcus suis serotype 2. *FEMS Immunol. Med. Microbiol.* **35,** 49–58.

Wahl, M., and Schilling, L. (1993). Regulation of cerebral blood flow—a brief review. *Acta Neurochir. Suppl. (Wien)* **59,** 3–10.

Wang, J., Rahman, M. F., Duhart, H. M., Newport, G. D., Patterson, T. A., Murdock, R. C., Hussain, S. M., Schlager, J. J., and Ali, S. F. (2009). Expression changes of dopaminergic system-related genes in PC12 cells induced by manganese, silver, or copper nanoparticles. *Neurotoxicology* **30,** 926–933.

Webb, A. A., and Muir, G. D. (2000). The blood-brain barrier and its role in inflammation. *J. Vet. Intern. Med.* **14,** 399–411.

Weber, S. J., Abbruscato, T. J., Brownson, E. A., *et al.* (1993). Assessment of an in vitro blood-brain barrier model using several [Met5]enkephalin opioid analogs. *J. Pharmacol. Exp. Ther.* **266,** 1649–1655.